Journal of Magnetism and Magnetic Materials 473 (2019) 221–227

Contents lists available at ScienceDirect

Journal of Magnetism and Magnetic Materials

journal homepage: www.elsevier.com/locate/jmmm

Research articles

Evidence of exchange coupling in τ-MnAlC/FeCo system

H. Martínez Sánchez[a,*], L.E. Zamora Alfonso[a], J.S. Trujillo Hernandez[a,b], G.A. Pérez Alcázar[a]

[a] Departamento de Física, Universidad del Valle, Meléndez, A.A. 25360, Cali, Colombia
[b] Facultad de Ciencias Naturales y Matemáticas, Universidad de Ibagué, Ibagué, Tolima, Colombia

ARTICLE INFO

Keywords:
Exchange coupling
Maximum energy product $(BH)_{max}$
Mechanical alloying
Sintering
X-ray diffraction (XRD)
Mössbauer spectroscopy (MS)

ABSTRACT

The τ-MnAlC/FeCo system has potential to be applied as rare earth-free permanent magnet, due to exchange coupled between hard and soft magnetic phases as alternative for the development of high energy product permanent magnets. In this work the hard-magnetic phase $Mn_{53.3}Al_{45}C_{1.7}$ ($\mu_0 H_c$ = 0.37 T of coercive force, M_r = 23.52 Am^2/kg of remanent magnetization, M_s = 52.94 Am^2/kg of saturation magnetization and $(BH)_{max}$ = 3.89 kJ/m^3 of maximum energy product) was mixed with the soft magnetic phase $Fe_{65}Co_{35}$ ($\mu_0 H_c$ = 0.007 T and M_s = 221.33 Am^2/kg) using a solid-state procedure. The magnetic materials were sintered using different ratios of hard and soft magnetic phases: 95:5, 90:10, 85:15 and 80:20; and different sintering temperatures (300, 400, 500 and 600 °C) in order to improve the magnetic properties. The magnetic exchange coupling between MnAlC and FeCo was proved by the hysteresis loop and its corresponding Thamm-Hesse analysis. The best result was obtained for MnAlC/FeCo (95/5 wt%) sintered at 500 °C during 30 min, for which the magnetic properties were $\mu_0 H_c$ = 0.277 T, M_s = 76.43 Am^2/kg and $(BH)_{max}$ = 5.57 kJ/m^3.

1. Introduction

Permanent magnetic materials with high performance are characterized by high magnetic anisotropy (K_u = 1.7 MJ/m^3), high Curie temperature ($T_c \sim 1000$ K) and a theoretical $(BH)_{max} \sim 110$ kJ/m^3 [1,2]. These class of materials are used for technological applications, consumer electronics, medical industry, transportation, alternative energy and others [2]. Due to this wide field of applications, hard magnetic materials have been receiving great scientific interest to improve their magnetic properties, specially focusing on rare earth (RE)-free magnets, due to the high prices of REs. Different processes have been implemented to obtain these new systems such as sintering, thermal treatments, refinement of grain size and others. These processes are the basis of the new exchange coupling model between hard and soft magnetic phases [3–12]. In this model, the magnetic properties are dependent on the intrinsic properties of both phases and it is proposed as an alternative solution to the issue of the high demand of RE free magnets.

The exchange coupling model developed, especially in magnetic films [13,14], suggests the preparation of nanocomposite magnets by coupling 85% of hard magnetic phase and 15% of soft magnetic phase. Recent work [15] proposes the τ-MnAl phase as a potential hard magnetic phase, because it has superior magnetic and mechanical properties than alnicos and hexaferrites permanent magnets [16]. The τ-MnAl is metastable phase with face centered tetragonal structure (fct), which is known in the literature as $L1_0$ [17,18]. The carbon addition helps to stabilize and increase the directional order along the [0 0 1] easy axis, which can lead to coercivity values between 2 and 3 kOe as already shown in Ref. [2]. Jian et al. [19] studied the microstructure and magnetic properties of alloys of $Mn_{53.3}Al_{45}C_{1.7}$ obtained by arc melting and ball milling, achieving stabilization of the ε-phase through annealing at 1373 K for 24 h followed by a low temperature annealing at 873 K for 30 min to obtain the τ-phase. The obtained phases were corroborated by XRD. By scanning electron microscopy (SEM), it was identified a continuous particle size reduction from 20 to 0.5 μm, and by vibrating sample magnetometry (VSM) it was seen a decrease in the saturation magnetization and an increase in the coercive field with the increase of the milling time.

For exchange coupling materials, the soft magnetic phase requires high magnetic permeability, high saturation magnetization and low coercivity [20]. The FeCo soft phase has recently been used for the exchange coupling with a hard-magnetic phase to increase the $(BH)_{max}$

* Corresponding author.
E-mail address: martinez.hugo@correounivalle.edu.co (H. Martínez Sánchez).

https://doi.org/10.1016/j.jmmm.2018.10.069
Received 13 June 2018; Received in revised form 14 October 2018; Accepted 15 October 2018
Available online 16 October 2018

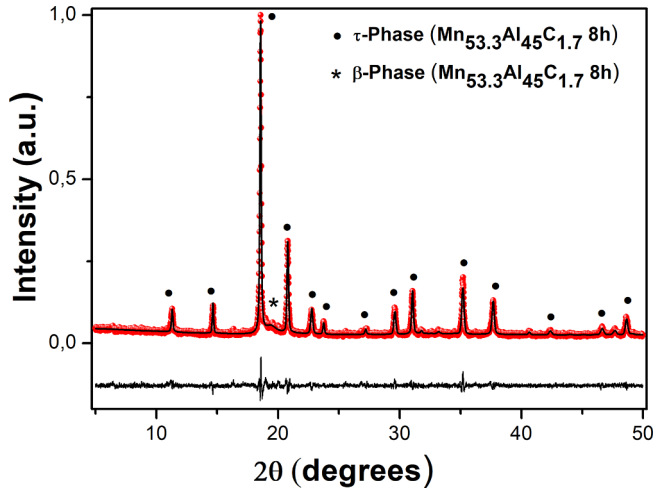

Fig. 1. X-ray pattern of the $Mn_{53.3}Al_{45}C_{1.7}$ sample milled for 8 h after annealed at 550 °C for 20 min.

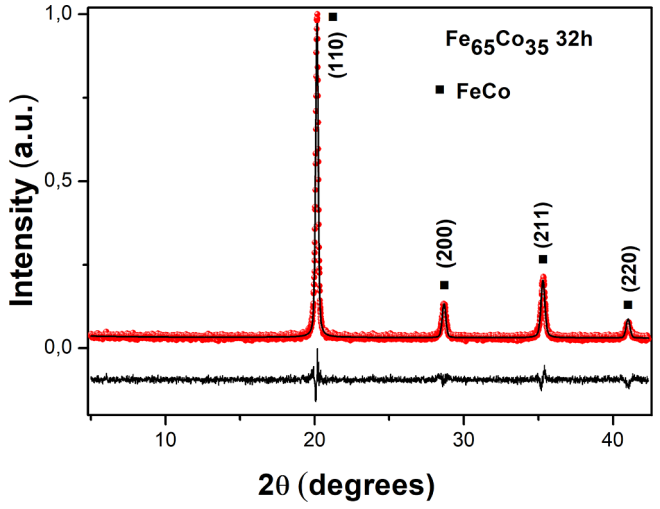

Fig. 2. X-ray pattern of $Fe_{65}Co_{35}$ milled for 32 h after annealed at 800 °C for 72 h.

in thin films. Dang et al. [21] studied the improvement of the $(BH)_{max}$ through the exchange coupling of thin films of MnAlC/FeCo, obtained by DC magnetron sputtering. They found an effective magnetic exchange coupling between MnAlC and FeCo thin films when the soft phase film thickness was less than 8 nm, and with this a significant improvement in the $(BH)_{max}$ was obtained. Recently, Trujillo et al. [22] studied the exchange coupling in nanocomposite magnets by milling melt-spun ribbon of $Mn_{54.3}Al_{44}C_{1.7}$ with α-Fe powders. They obtained the hard phase and optimized it after a heat treatment at 500 °C for 20 min. The mixture between τ-$Mn_{54.3}Al_{44}C_{1.7}$ and α-Fe phases showed, by XRD, a decrease in the τ-phase peaks. The nanocomposite sintering between 500 and 600 °C showed a decreasing tendency of the coercivity and the increase of the saturation magnetization. The evidence of the exchange coupling between the particles was studied by the Thamm-Hesse analysis [23] of the hysteresis loops.

Recent works have shown that the τ-MnAl hard magnetic phase optimization depends on the production method and thin films are the focus of recent works. Until now, researchers are working on the optimization of the τ-MnAl phase mixed with a soft phase through the exchange coupling in bulk samples, implementing mechanical alloying, sintering and other techniques. The main goal in this work is to obtain a magnetic exchange-coupling between hard magnetic (τ-MnAlC) and soft magnetic (FeCo) phases to improve the energy-product. For this reason, in this study, we propose to improve the magnetic properties of bulk nanocomposite magnets by optimizing the exchange coupling between the τ-$Mn_{53.3}Al_{45}C_{1.7}$ hard magnetic phase and the $Fe_{65}Co_{35}$ soft magnetic phase. The study by mechanical alloying and sintering, mixing 5 to 20% in mass of the soft phase, were performed to optimize the magnetic properties focused on RE-free permanent magnet, that can be used in the different applications mentioned above.

2. Materials and methods

$Mn_{53.3}Al_{45}C_{1.7}$ and $Fe_{65}Co_{35}$ alloys have been obtained by melt spinning and arc melting, respectively, from high purity elements. The FeCo alloy was annealed at 800 °C by 72 h and then quenched in water to homogenize and stabilize the α (A2) phase of FeCo which is disordered at that temperature according to its phase diagram. This phase presents a soft magnetic behavior. After the heat treatment, mechanical alloying was carried out for 32 h assisted with oleic acid to reduce the particle size and improve its soft magnetic behavior. MnAlC alloy was obtained by melt spinning. 3 wt% of Mn in excess was added to compensate its evaporation during the melting process. The ribbons presented only hexagonal ε-MnAl phase, in accordance with previous reports [22]. After that, the ribbons were annealed at 550 °C for 20 min to stabilize the τ-MnAl tetragonal phase; finally, the sample was ball milled for 8 h at 150 rpm to reduce the particle size and increase the coercivity value. Finally, the soft and hard phases were mixed at mass percentages of 5, 10, 15 and 20% of FeCo. Then the mixtures were homogenized for 1 h by mechanical alloying at low energy (150 RPM). Further, they were compacted to 75 kN of pressure and sintered at 300, 400, 500 and 600 °C for 30 min.

The samples were characterized by X-Ray Diffraction (XRD) carried out on a Stoe Stadi P diffractometer with Mo $K_{\alpha 1}$ radiation, in transmission geometry, in the 2θ range between 5 and 50°; Vibrating sample magnetometry (VSM) with an applied external field of 2 and 3 T for the soft and hard phases, respectively. Demagnetization correction was made for the magnetic measurements. The Thamm-Hesse method was used to study the type of predominant interactions between particles. In order to evaluate the magnetic interaction, we use a simple relation, which is called the ΔM-plot, $\Delta M = M_{init} - (1/2) \times (M_{up} + M_{down})$, where the M_{init}, M_{up}, and M_{down} are the magnetization values over the initial magnetization curve, upper, and lower part of the hysteresis loop, respectively, as described in Ref. [23]. Scanning Electron

Table 1
XRD parameters of $Mn_{53.3}Al_{45}C_{1.7}$ and $Fe_{65}Co_{35}$ samples.

Sample	Phase	Lattice parameter [Å] ± 0.001	Crystallite size		Weight fraction	Density (g/cm^3)
			$\Phi_{\parallel}$ [nm] ± 0.05	$\Phi_{\perp}$ [nm] ± 0.05		
$Mn_{53.3}Al_{45}C_{1.7}$	τ	a = 3.921 c = 3.586	347.68	627.05	85	5.27
	β	a = 6.906	233.56	123.11	15	5.53
$Fe_{65}Co_{35}$	α (A_2)	a = 2.860	184.58	431.01	100	8.85

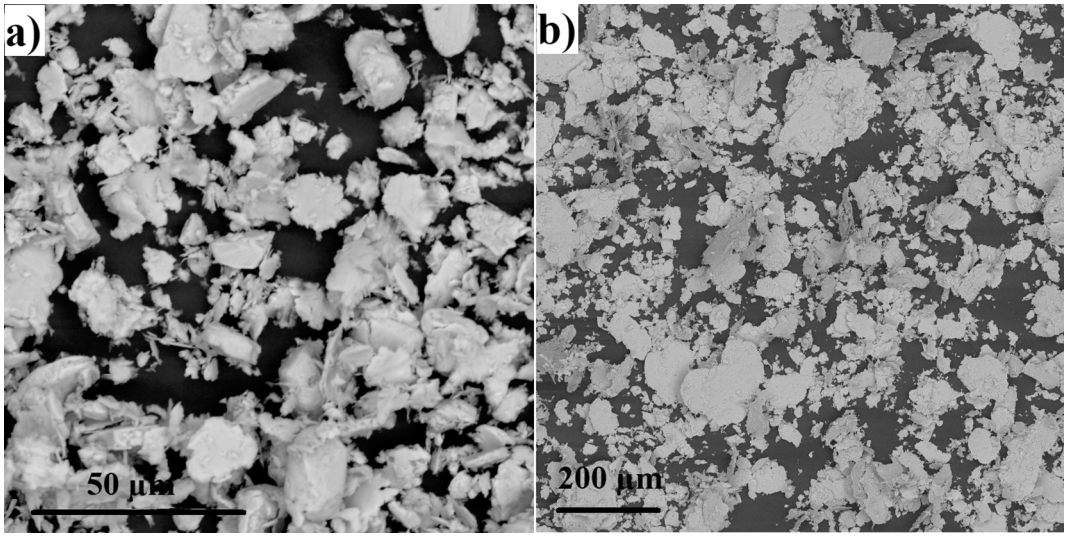

Fig. 3. SEM images of (a) $Mn_{53.3}Al_{45}C_{1.7}$, and (b) $Fe_{65}Co_{35}$.

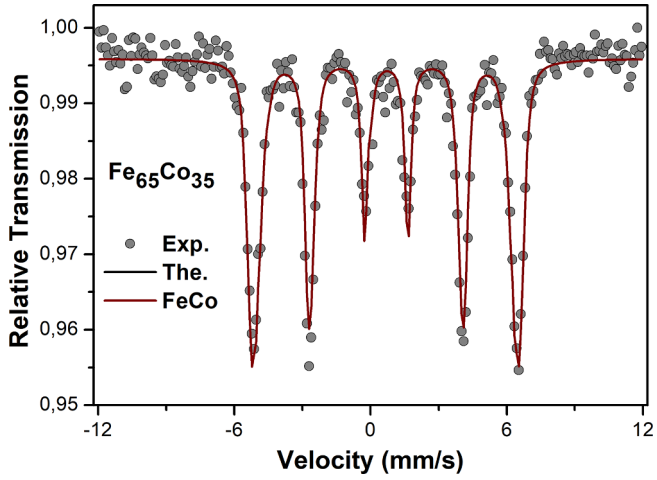

Fig. 4. Mössbauer spectrum of $Fe_{65}Co_{35}$ milled for 32 h after annealed at 800 °C.

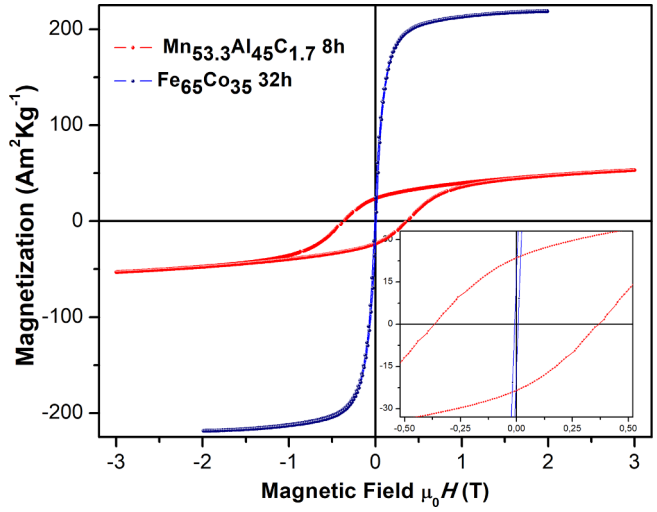

Fig. 5. Hysteresis loops of $Fe_{65}Co_{35}$ milled for 32 h and $Mn_{53.3}Al_{45}C_{1.7}$ milled for 8 h after annealed.

Microscopy (SEM) was taken in the range between 20 and 200 µm for each sample; and Mössbauer Spectroscopy (MS) at room temperature, using a Mössbauer spectrometer with a radioactive source of ^{57}Co immersed in a rhodium (Rh) matrix. XRD diffraction patterns were refined with the GSAS software [24], the Mössbauer spectrum of the soft phase was adjusted with the Mosfit program [25], and the average particle size was obtained from SEM images, using the GIMP and ImageJ programs.

3. Results and discussion

The constitution of the $Mn_{53.3}Al_{45}C_{1.7}$ hard phase alloy was determined by XRD as shown in Fig. 1. Both τ and β phases are present; the τ-phase, with the space group *P4/mmm*, presents a tetragonal crystallographic structure with lattice parameters $a = 3.9207$ Å and $c = 3.5860$ Å, with average crystallite sizes ($\Phi_{\parallel}$ *parallel and* $\Phi_{\perp}$ *perpendicular*) of $\Phi_{\parallel} = 347.68$ nm and $\Phi_{\perp} = 627.05$ nm indicating that on average the crystallites are prolate. The τ-phase has a weight fraction of 85% and constitutes the hard-magnetic phase.

The coexistence of the β phase with a weight fraction of 15% was also observed. This phase has a P4132 space group, which is a simple cubic structure with lattice parameter $a = 6.9064$ Å and average crystallite sizes of $\Phi_{\parallel} = 233.56$ nm and $\Phi_{\perp} = 123.11$ nm indicating that on average the crystallites are prolate; phase β has been indexed with an asterisk as shown in Fig. 1.

Fig. 2 shows the X-ray diffraction pattern of the $Fe_{65}Co_{35}$ sample milled with surfactant for 32 h, and then annealed at 800 °C. The preparation route retains the bcc structure of FeCo alloy with the *Im3m* space group. This pattern was refined with the CIF (Crystallographic Information File) of the $Co_{0.18}Fe_{1.82}$ phase. The refined lattice parameter was $a = 2.8604$ Å, and the refined mean crystallite sizes were

Table 2
Main parameters corresponding to hysteresis loop for $Mn_{53.3}Al_{45}C_{1.7}$ and $Fe_{65}Co_{35}$ samples.

Sample	M_s ($Am^2 kg^{-1}$) ± 0.05	M_r ($Am^2 kg^{-1}$) ± 0.05	H_c $\mu_0 H$ (T) ± 0.003	$(BH)_{max}$ ($kJ m^{-3}$)
$Mn_{53.3}Al_{45}C_{1.7}$	52.94	23.52	0.370	3.89
$Fe_{65}Co_{35}$	221.33	17.88	0.007	–

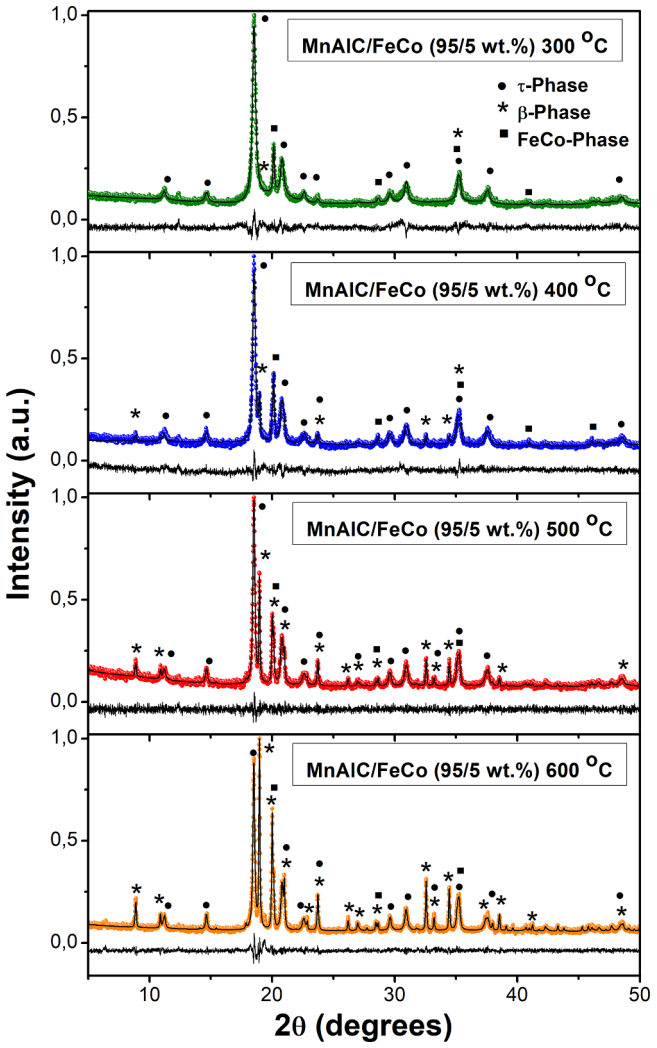

Fig. 6. X-ray patterns of MnAlC/FeCo (95/5 wt%) sample sintered at 300, 400, 500 and 600 °C during 30 min.

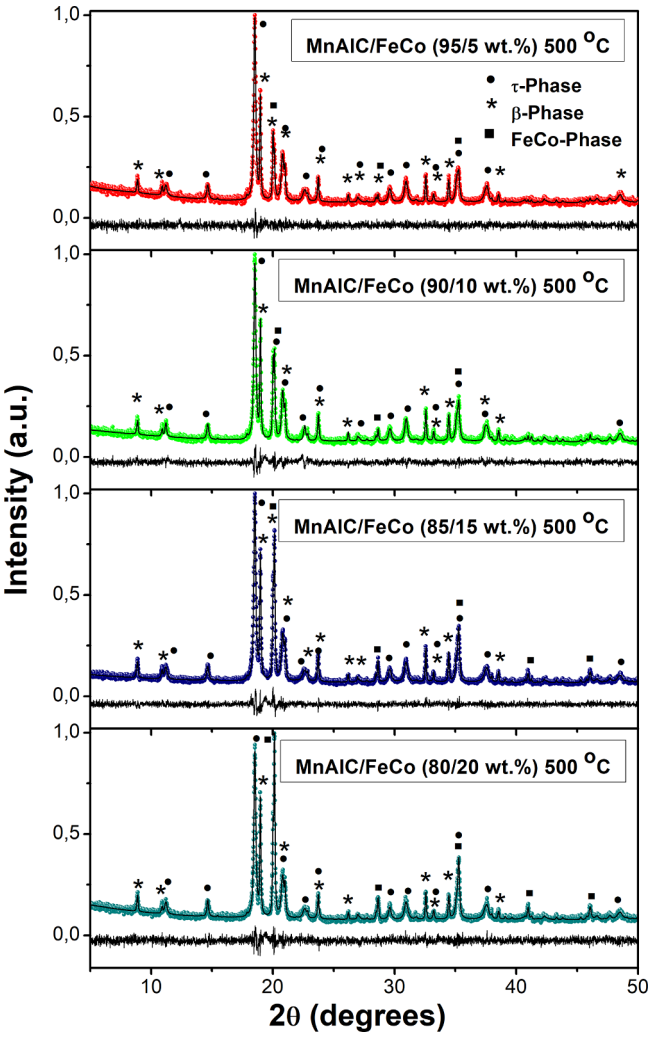

Fig. 7. X-ray patterns of MnAlC/FeCo at 500 °C, for concentrations of 5, 10, 15 and 20% of the soft phase.

Table 3
X-ray diffraction parameters of MnAlC/FeCo (95/5 wt%) sample sintered at 300, 400, 500 and 600 °C.

Sample	Phase	Lattice parameter [Å] ± 0.001	Crystallite size		Weight fraction	Density (g/cm^3)
			$\Phi_{\parallel}$ [nm] ± 0.05	$\Phi_{\perp}$ [nm] ± 0.05		
MnAlC/FeCo (95/5 wt%) 300 °C	τ	a = 3.921 c = 3.614	120.04	120.04	67	4.94
	β	a = 5.942	717.17	24.50	28	8.69
	α (A_2)	a = 2.856	222.55	442.70	5	7.60
MnAlC/FeCo (95/5 wt%) 400 °C	τ	a = 3.918 c = 3.608	210.91	190.10	67	5.01
	β	a = 6.446	395.12	395.12	10	6.77
	α (A_2)	a = 2.865	30.10	276.88	23	7.93
MnAlC/FeCo (95/5 wt%) 500 °C	τ	a = 3.922 c = 3.612	228.74	226.34	70	4.85
	β	a = 6.446	600.49	600.49	24	6.19
	α (A_2)	a = 2.867	269.73	365.39	6	7.91
MnAlC/FeCo (95/5 wt%) 600 °C	τ	a = 3.919 c = 3.616	403.26	246.14	51	4.89
	β	a = 6.444	325.15	468.71	44	5.37
	α (A_2)	a = 2.863	199.51	527.56	5	7.95

Table 4
X-ray diffraction parameters of MnAlC/FeCo (90/10, 85/15, and 80/20 wt%) samples sintered at 300, 400, 500 and 600 °C.

Sample	Phase	Lattice parameter [Å] ± 0.001	Crystallite size		Weight fraction	Density (g/cm^3)
			$\Phi_{\parallel}$ [nm] ± 0.05	$\Phi_{\perp}$ [nm] ± 0.05		
MnAlC/FeCo (90/10 wt%) 500 °C	τ	a = 3.919 c = 3.610	262.95	262.95	63	4.91
	β	a = 6.442	340.30	496.01	27	6.57
	α (A_2)	a = 2.865	315.06	356.49	10	7.92
MnAlC/FeCo (85/15 wt%) 500 °C	τ	a = 3.925 c = 3.616	345.71	268.34	62	4.77
	β	a = 6.443	383.67	422.25	25	6.44
	α (A_2)	a = 2.865	521.02	521.02	13	7.93
MnAlC/FeCo (80/20 wt%) 500 °C	τ	a = 3.923 c = 3.613	399.30	399.30	56	4.89
	β	a = 6.443	376.06	481.01	26	6.50
	α (A_2)	a = 2.865	581.41	579.56	18	7.45

$\Phi_{\parallel}$ = 18 nm and $\Phi_{\perp}$ = 43 nm indicating that on average the crystallites are prolate. In addition, the obtained XRD parameters of the $Mn_{53.3}Al_{45}C_{1.7}$ and $Fe_{65}Co_{35}$ samples are listed in Table 1.

Fig. 3 shows SEM images of the $Mn_{53.3}Al_{45}C_{1.7}$ (a), and $Fe_{65}Co_{35}$ (b) samples. The micrographic analysis shows an average particle diameter between 7 and 14 μm for (a), and (b), respectively. It can be seen that the milling time reduces the particle size and promote micro flakes with irregular shape.

The Mössbauer spectrum of $Fe_{65}Co_{35}$ milled for 32 h is shown in Fig. 4. The six lines indicate a magnetic behavior, and their high broad show that the crystalline sample is disordered and Fe are randomly substituted by Co atoms. This fact permits to conclude that the obtained bcc structure corresponds to the disordered α (A2) phase. The best fit, and in accord with its disordered character, was obtained with a hyperfine magnetic field distribution (HMFD) with a mean hyperfine field of $\langle B \rangle$ = 35.6 T. The increase of $\langle B \rangle$, respect the 32 T of the pure Fe, is due to the substitution of Fe atoms by magnetic Co atoms. These results are in accord with those of Zelenaková et al. [26], which reported the Mössbauer study of $Fe_{70}Co_{30}$ obtained by mechanical alloying for 30 h, and determined a field of $\langle B \rangle$ = 35 T.

Fig. 5 shows hysteresis loops of $Mn_{53.3}Al_{45}C_{1.7}$ and $Fe_{65}Co_{35}$ identified as hard and soft magnetic phases, respectively. $Mn_{53.3}Al_{45}C_{1.7}$ presents $\mu_0 H_c$ = 0.370 T, M_r = 23.52 Am^2/kg, M_s = 52.94 Am^2/kg for an applied field of 3 T and a $(BH)_{max}$ = 3.89 kJ/m^3. On the other hand the $Fe_{65}Co_{35}$ presents $\mu_0 H_c$ = 0.007 T, M_r = 18.17 Am^2/kg and M_s = 221.33 Am^2/kg. A summary of the main parameters corresponding to the hysteresis loops for $Mn_{53.3}Al_{45}C_{1.7}$ and $Fe_{65}Co_{35}$ samples are included in Table 2.

After the characterization of the $Mn_{53.3}Al_{45}C_{1.7}$ and $Fe_{65}Co_{35}$ phases, they were mixed in mass percentages from 5 to 20% of soft phase and a mass percent from 95 to 80% of hard phase, respectively. The different mixtures were denoted as MnAlC/FeCo (95/5 wt%), MnAlC/FeCo (90/10 wt%), MnAlC/FeCo (85/15 wt%) and MnAlC/FeCo (80/20 wt%). After this, the mixtures were homogenized by mechanical alloying, and compacted at a pressure of 75 kN. To determine the optimal sintering temperature, the sample MnAlC/FeCo (95/5 wt%) was taken and heat treated at 300, 400, 500 and 600 °C during 30 min. After the mixture of soft and hard magnetic phases, the samples were characterized structurally and magnetically. The X-ray diffraction patterns of the MnAlC/FeCo sample (95/5 wt%) at temperatures between 300 and 600 °C, are shown in Fig. 6.

Diffraction patterns at the different thermal treatment temperatures reveal the presence of τ, β and α-FeCo phases, which are hard ferromagnetic, paramagnetic and soft ferromagnetic, respectively. The increase of the β phase fraction, observed by XRD, indicates that this phase is favored by the increase in temperature, as shown in Fig. 6. A summary of the obtained XRD parameters of the MnAlC/FeCo (95/5 wt %) at different temperatures are listed in Table 3.

Taken into account the optimized sintering temperature of 500 °C, the hard and soft phase samples of 90:10, 85:15 and 80:20 wt% were sintered in this condition. Fig. 7 shows the diffraction patterns of the samples sintered at 500 °C during 30 min for the different hard and soft phase compositions.

The XRD patterns present the same three crystallographic phases: τ,

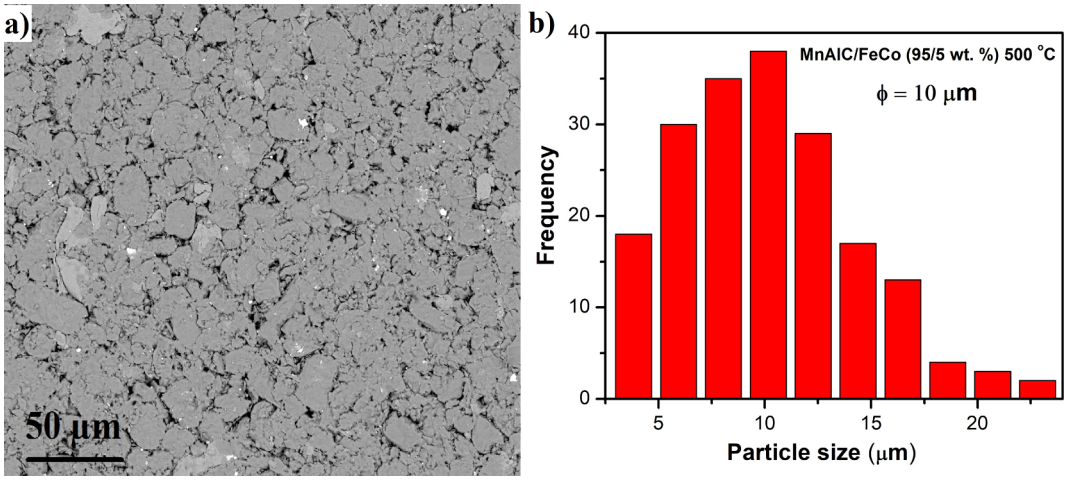

Fig. 8. (a) SEM images of MnAlC/FeCo (95/5 wt%) at 500 °C, and (b) Distribution of the average particle size of MnAlC/FeCo (95/5 wt%) at 500 °C.

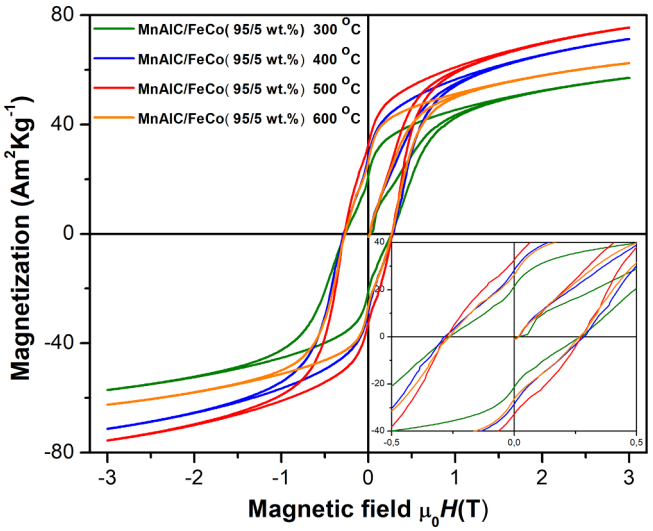

Fig. 9. Hysteresis loops of MnAlC/FeCo (95/5 wt%) sintered at 300, 400, 500 and 600 °C during 30 min.

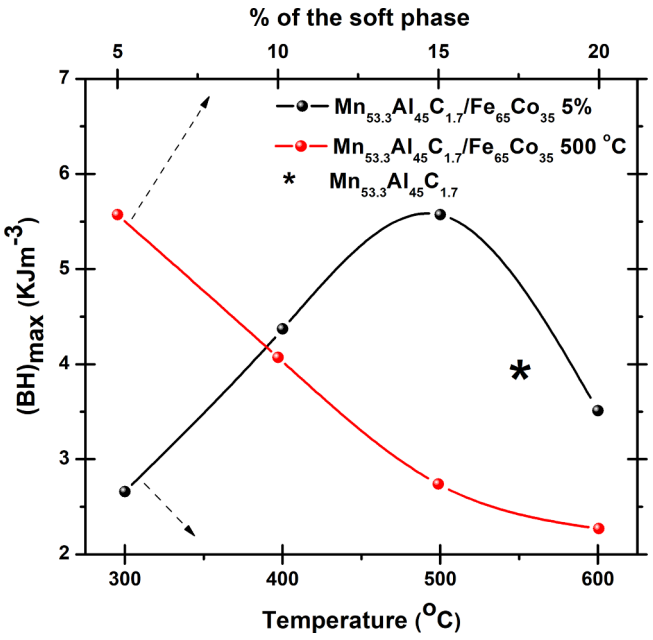

Fig. 10. $(BH)_{max}$ as a function of temperature and % of the soft phase of MnAlC/FeCo sintered at 300, 400, 500, and 600 °C, for the soft mass percentages of 5, 10, 15 and 20%.

β and α-FeCo. The weight fraction of the α-FeCo phase increases from 6 to 18% due to the increase of mass percent of the soft phase in the sample from 5 to 20%. These increase is noted by the increase of the intensity of the main peaks of α-FeCo phase, as shown in Fig. 7. On the other hand, the τ-phase decreases its weight fraction in the sample from 70 to 56%, and the β phase increases its weight fraction with the

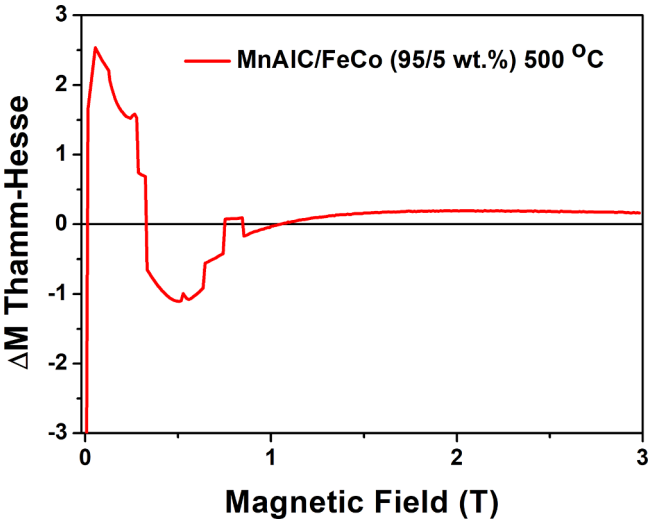

Fig. 11. The Thamm-Hesse plot of MnAlC/FeCo (95/5 wt%) sintered at 500 °C.

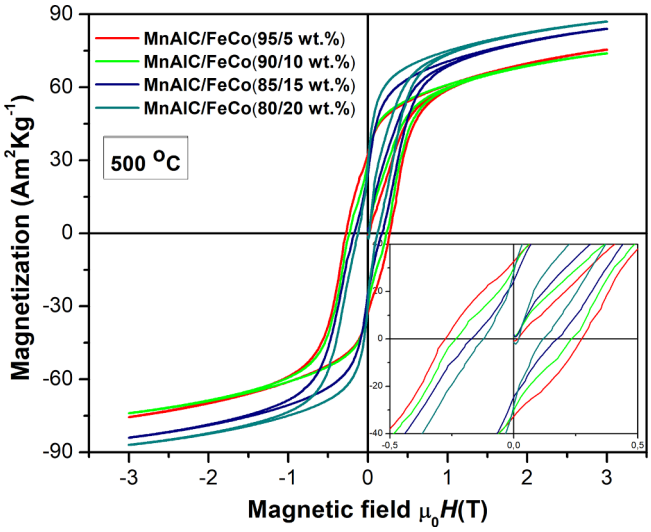

Fig. 12. Hysteresis loops of MnAlC/FeCo sintered at 500 °C, for mass percentages of 5, 10, 15 and 20% of the soft phase.

increase of the soft phase. A summary of the obtained XRD parameters of the MnAlC/FeCo with different ratios at 500 °C are listed in Table 4.

Fig. 8(a) shows SEM images of the MnAlC/FeCo (95/5 wt%) at 500 °C samples. The micrographic analysis shows an average particle diameter of 10 μm respectively. In Figure it can be observed white and gray particles, the first corresponding to the soft phase. If we compare the obtained mean particle sizes with the mean crystallite sizes obtained by the Rietveld refinement, it can be concluded that the soft and hard particles are polycrystalline. The distribution of the average particle diameter or average particle size of MnAlC/FeCo (95/5 wt%) at 500 °C is shown in Fig. 8(b). It can be noted that the probably particle size is near 10 μm.

Table 5
Magnetic properties of MnAlC/FeCo (95/5 wt%) sample sintered at 300, 400, 500 and 600 °C during 30 min.

Sample	M_s (Am^2kg^{-1}) ± 0.05	M_r (Am^2kg^{-1}) ± 0.05	H_c μ_0H (T) ± 0.003	$(BH)_{max}$ (kJm^{-3})
MnAlC/FeCo (95/5 wt%) 300 °C	57.73	21.41	0.270	2.66
MnAlC/FeCo (95/5 wt%) 400 °C	71.61	28.31	0.285	4.37
MnAlC/FeCo (95/5 wt%) 500 °C	76.43	32.71	0.277	5.57
MnAlC/FeCo (95/5 wt%) 600 °C	62.72	26.31	0.264	3.51

Table 6
Magnetic properties of MnAlC/FeCo (90/10, 85/15, and 80/20 wt%) sample sintered at 500 °C during 30 min.

Sample	M_s ($Am^2 kg^{-1}$) ± 0.05	M_r ($Am^2 kg^{-1}$) ± 0.05	H_c $\mu_0 H$ (T) ± 0.003	$(BH)_{max}$ ($kJ m^{-3}$)
MnAlC/FeCo (90/10 wt%) 500 °C	74.75	30.15	0.234	4.07
MnAlC/FeCo (85/15 wt%) 500 °C	84.21	24.76	0.173	2.74
MnAlC/FeCo (80/20 wt%) 500 °C	87.52	28.33	0.122	2.27

Fig. 9 shows hysteresis loops of MnAlC/FeCo (95/5 wt%) sample sintered at 300, 400, 500 and 600 °C during 30 min. In Fig. 9 it can be seen that the hysteresis loop of the sample sintered at 500 °C, showed characteristic behavior of a single-phase hard magnet with no kinks in the demagnetization curve, consistent with the existence of strong intergrain exchange coupling between MnAlC/FeCo phases. The magnetic properties $M_s = 76.43\ Am^2/kg$, $M_r = 32.71\ Am^2/kg$, $\mu_0 H_c = 0.277$ T and $(BH)_{max} = 5.57\ kJ/m^3$, were achieved in this sample, which are higher compared to those of the standard sample ($Mn_{53.3}Al_{45}C_{1.7}$), and the other evaluated mixture ratios at different temperatures. It is important to note that $(BH)_{max}$ is directly related to the weight fraction of phase τ in the samples (see Fig. 10). A summary of the main parameters corresponding to the hysteresis loop of MnAlC/FeCo (95/5 wt%) sample sintered at 300, 400, 500 and 600 °C during 30 min, are included in Table 5.

The Thamm-Hesse plot (Fig. 11) was obtained from the hysteresis loop at room temperature as described in Ref. [23]. Here, the Thamm-Hesse method was used to establish the type of magnetic interaction existing between magnetic particles according to the ΔM parameter. For $\Delta M \neq 0$, there are interactions between the particles or grains. In the case that $\Delta M > 0$, interactions that favor magnetization prevail (exchange interaction), but if $\Delta M < 0$, the interactions that prevail are those that favor magnetization reversal (dipolar interaction) [23]. Then for the nanostructured composite τ-MnAlC/FeCo samples, the data show a peak splitting in the Thamm-Hesse plots. This analysis shows a competition between the magnetic dipolar interaction and the exchange interaction occurs; however, the last one predominates. This behavior suggests that within the material, there is an intimate ferromagnetic exchange coupling between particles of the hard τ-MnAlC phase and between them with those of the soft FeCo. This result is according with Trujillo et al. [22]. This is a consequence of the grain size refinement produced by milling process with surfactant and the increase of the FeCo content.

The Fig. 12 shows hysteresis loops of MnAlC/FeCo (95/5, 90/10, 85/15, and 80/20 wt%) samples sintered at 500 °C during 30 min. In Fig. 12 it can be seen that the magnetic properties of the sample sintered at 500 °C, began to decrease with the increase in FeCo content. This is the reason of the decrease of $(BH)_{max}$ from $5.57\ kJ/m^3$ for the MnAlC/FeCo (95/5 wt%) sample to $2.27\ kJ/m^3$ for the MnAlC/FeCo (80/20 wt%) sample, as can be observed in the Table 6.

4. Conclusions

The structural and magnetic properties of the $Mn_{53.3}Al_{45}C_{1.7}$ hard phase, the $Fe_{65}Co_{35}$ soft phase and their mixtures in mass percentages of 95:5, 90:10, 85:15 and 80:20 of the hard and soft phases were studied. The sample MnAlC/FeCo (95/5 wt%) sintered at 500 °C during 30 min reveals an exchange coupling between its precursor phases, presenting the best hard magnetic properties with $(BH)_{max} = 5.57\ kJ/m^3$. The decrease in $(BH)_{max}$ is related to the decrease of weight fraction of the percentage of τ phase in the sample. The increase of the mass percentage of the soft phase from 5 to 20% increase the M_s and decrease the $\mu_0 H_c$ of the mixture compared to the M_s and $\mu_0 H_c$ of the $Mn_{53.3}Al_{45}C_{1.7}$ hard phase. Evidence of good exchange coupling between τ-MnAlC/FeCo is observed by Thamm-Hesse, but future experiments are necessary to optimize processing of the particle size reduction.

Acknowledgments

The authors would like to thanks Colciencias (Colombian Agency) and the Vicerrectoría de Investigaciones of the Universidad del Valle for the support with the Young Researches program-Convocatoria 761-2016, given to HMS. To COLCIENCIAS, under Contract 110671250407, and especially to INAPEM (International Network on Applications of Permanent Magnets) (project EU 691235) for kind support to our research group.

References

[1] P. Nieves, Atomistic spin dynamics simulations of the MnAl τ-phase and its anti-phase boundary, Phys. Rev. B 96 (224411) (2017) 1–10.
[2] G.A.P. Alcázar, Imanes permanentes: características, aplicaciones y futuro, Rev. Acad. Colomb. Ciencias Exactas, Físicas y Nat. 40 (2016) 221–233.
[3] R.C. O'handley, Moder, Magnetic Materials Principles and Applications, Wiley, New York, 2000.
[4] E.F. Kneller, R. Hawig, The exchange-spring magnet: A new material principle for permanent magnet magnets, IEEE Trans. Magn. 27 (1991) 3588–3600.
[5] R. Fischer, T. Leineweber, H. Kronmüller, Fundamental magnetization processes in nanoscaled composite permanent magnets, Phys. Rev. B 57 (1998) 10723–10732.
[6] T.X. Nguyen, Enhancement of exchange coupling interaction of NdFeB/MnBi hybrid magnets, Phys. B: Condens. Matter 532 (2018) 130–134.
[7] M. Pousthomis, On the advantages of spring magnets compared to pure FePt: strategy for rare-earth free permanent magnets following a bottom-up approach, J. Magn. Magn. Mater. 424 (2017) 304–313.
[8] W. Cui, $Nd_2Fe_{14}B$/FeCo anisotropic nanocomposite films with a large maximum energy product, Adv. Mater. 24 (2012) 6530–6535.
[9] A.L. Wysocki, Micromagnetic simulations with periodic boundary conditions: hard-soft nanocomposites, J. Magn. Magn. Mater. 428 (2017) 274–286.
[10] A.L. Ortega, M. Estrader, G.S. Alvarez, A.G. Roca, J. Nogués, Applications of exchange coupled bi-magnetic hard/soft and soft/hard magnetic core/shell nanoparticles, Phys. Rep. 553 (2015) 1–32.
[11] H. Zeng, J. Li, J.P. Liu, Z.L. Wang, S. Sun, Exchange-coupled nanocomposite magnets by nanoparticle self-assembly, Nature 420 (2002) 395–398.
[12] X.Q. Liu, S.H. He, J.P. Wang, Nanocomposite exchange-spring magnet synthesized by gas phase method: from isotropic to anisotropic, Appl. Phys. Lett. 98 (222507) (2011) 1–3.
[13] E.E. Fullerton, J.S. Jiang, S.D. Bader, Hard/soft magnetic heterostructures: model exchange-spring magnets, J. Magn. Magn. Mater. 200 (1999) 392–404.
[14] L.H. Lewis, F.J. Villacorta, Perspectives on permanent magnetic materials for energy conversion and power generation, Metall. Mater. Trans. A 44 (2013) 2–20.
[15] M.J. Lucis, T.E. Prost, X. Jiang, M. Wang, J.E. Shield, Phase transitions in mechanically milled Mn-Al-C permanent magnets, Metals 4 (2014) 130–140.
[16] L.G. Marshall, I.J. McDonald, L.H. Lewis, Quantification of the strain-induced promotion of τ-MnAl via cryogenic milling, J. Magn. Magn. Mater. 404 (2016) 215–220.
[17] H. Kono, On the ferromagnetic phase in manganese-aluminum system, J. Phys. Soc. Jpn. 13 (1958) 444–1451.
[18] J.M.D. Coey, New permanent magnets; manganese compounds, Condens. Matter 26 (2014) 1–6.
[19] H. Jian, K.P. Skokov, O. Gutfleisch, Microstructure and magnetic properties of Mn-Al-C alloy powders prepared by ball milling, J. Alloys Compd. 622 (2015) 524–528.
[20] D. Jiles, Introduction to Magnetism and Magnetic Materials, first ed., (1991).
[21] R. Dang, X. Ma, J. Liu, Y. Zhang, S. Qian, The fabrication and characterization of MnAl/FeCo composite thin films with enhanced maximum energy products, Mater. Lett. 197 (2017) 8–11.
[22] J.S.T. Hernandez, F. Maccari, L.G. Marshall, J.A. Tabares, G.A.P. Alcázar, Exchange coupling in MnAlC/α-Fe nanocomposite magnets, J. Supercond. Nov. Magn. 31 (2018) 1–7.
[23] S. Thamm, J. Hesse, A simple plot indicating interactions between single-domain particles, J. Magn. Magn. Mater. 154 (1996) 254–262.
[24] A.C. Larson, R.B. Von Dreele, General Structure Analysis System (GSAS), Los Alamos National Laboratory Report LAUR (2004) 86–748.
[25] J. T. F. Varret, Unpubl. Mosfit Program, Univ. du Maine, Le Mans, Fr. (n.d.).
[26] A. Zeleňáková, D. OlekšáKová, J. Degmová, J. Kováč, P. Kollár, M. Kúsý, P. Sovák, Structural and magnetic properties of mechanically alloyed FeCo powders, J. Magn. Magn. Mater. 316 (2007) 3–6.